

N69-35768
NASA CR-105427

VLF MEASUREMENTS
OF THE POYNING FLUX ALONG
THE GEOMAGNETIC FIELD WITH
THE INJUN 5 SATELLITE*

Stephen R. Mosier**
Donald A. Gurnett



CASE FILE
COPY

Department of Physics and Astronomy
THE UNIVERSITY OF IOWA

Iowa City, Iowa

VLF MEASUREMENTS
OF THE POYNTING FLUX ALONG
THE GEOMAGNETIC FIELD WITH
THE INJUN 5 SATELLITE*

Stephen R. Mosier**
Donald A. Gurnett

Department of Physics and Astronomy
The University of Iowa
Iowa City, Iowa

June 1969

*Research supported in part by the National Aeronautics and Space Administration under Contracts NAS5-10625, NAS1-8141, NAS1-8144(f), NAS1-8150(f), and NGR-16-001-043; and by the Office of Naval Research under Contract Nonr 1509(06).

**Graduate Trainee of the National Aeronautics and Space Administration.

ABSTRACT

The direction of the Poynting flux, up or down the geomagnetic field, has been determined for several types of VLF radio noise phenomena observed with the Injun 5 satellite, thereby providing information about the source region of these waves and their propagation in the ionosphere. Determinations of the Poynting flux direction of proton whistlers show that they are propagating up the geomagnetic field lines in accordance with the accepted theory of proton whistler propagation, thus providing a good check on the experimental technique. Initial measurements are presented on the Poynting flux direction of ELF hiss, periodic emissions, VLF hiss, and chorus. Of particular interest is a new type of VLF emission called a saucer which is found to be propagating upward from a source below the satellite. A qualitative explanation of the frequency-time shape of this new type of emission is presented.

I. INTRODUCTION

Although there exists a considerable body of data on magnetospheric VLF radio noises [see, for example, Helliwell, 1965], no direct measurements have been made to determine the source region of these noises. Since the emission mechanisms are usually very dependent on the plasma parameters in the source region, it is of fundamental importance to establish the source region of these noises, particularly whether the noises are generated at low altitudes near the base of the ionosphere or at much higher altitudes in the magnetosphere. This paper presents initial results on measurements of the Poynting flux direction, up or down the geomagnetic field, of VLF electromagnetic waves in the frequency range from 30 Hz to 10 kHz using the NASA/University of Iowa Injun 5 satellite.

The Injun 5 satellite was launched on 8 August 1968 into an elliptical polar orbit with an inclination of 80.66°, an apogee altitude of 2528 km, and a perigee altitude of 677 km. The satellite carried a VLF experiment, which is described in more detail by Gurnett et al. [1969], consisting of one electric dipole antenna, one magnetic loop antenna, two wide-band (30 Hz to 10 kHz) receivers, a narrow-band step-frequency receiver, and an impedance measurement for

determining the electric antenna impedance. The spacecraft is magnetically oriented by a bar magnet in the spacecraft such that the x-axis of the spacecraft is parallel to the geomagnetic field (see Figure 1), with the positive x-axis downward in the northern hemisphere. Typical maximum alignment errors between the x-axis and the geomagnetic field after about mid-December, 1968, when magnetic alignment was achieved, are about 10 to 15 degrees. When magnetically oriented the electric antenna axis (y-axis) and the magnetic antenna axis (z-axis) are perpendicular to the geomagnetic field, as well as to each other (see Figure 1). As discussed in the next section, this antenna geometry has the feature that the direction of the Poynting flux, up or down the geomagnetic field, can be determined from the time-averaged product $\langle E_y B_z \rangle$ of the electric and magnetic antenna signals.

III. METHOD AND LIMITATIONS OF THE POYNTING FLUX MEASUREMENT

For a single plane wave propagating in a cold plasma at a frequency less than the electron plasma frequency, it can be shown [Gurnett et al, 1969] that the sign of the time-averaged product $\langle E_y B_z \rangle$, where E_y and B_z are orthogonal electric and magnetic field components in a plane perpendicular to the static magnetic field, is the same as the sign of the time-averaged component of the Poynting flux $\langle S_x \rangle$ along the static magnetic field. For the Injun 5 orbit, the frequencies of interest (30 Hz to 10 kHz) are normally much less than the electron plasma frequency. Thus, for a single wave, the measurement of $\langle E_y B_z \rangle$ with Injun 5 is sufficient to determine whether the Poynting flux of the wave is directed up or down the geomagnetic field.

If a superposition of many waves is observed, then this interpretation must be qualified. Since the proportionality between $\langle E_y B_z \rangle$ and $\langle S_x \rangle$ for a single wave depends upon the wave normal direction [see Gurnett et al, 1969], and since the wave normal directions of the various waves are in general different, the time average $\langle E_y B_z \rangle$ for a superposition of many waves is not necessarily proportional to the average Poynting flux $\langle S_x \rangle$ of all the waves. Under these conditions the interpretation which can be made is as

follows: if the sign of $\langle E_y B_z \rangle$ is observed to be positive, then at least some of the waves must have a Poynting flux in the positive x direction. However, there may also be waves with Poynting fluxes in the negative x direction and the relative intensity of these waves cannot be determined without further information on the wave normal angles involved. Similar statements hold when the sign of $\langle E_y B_z \rangle$ is negative. A measurement of $\langle E_y B_z \rangle$ with Injun 5 therefore allows one to make a positive statement that some waves are propagating in a certain direction, up or down the geomagnetic field; but it does not deny the possibility that there may also be waves propagating in the opposite direction.

Possible errors in the Poynting flux determinations can arise whenever the electric (y) and magnetic (z) antenna axes are not aligned exactly perpendicular to the geomagnetic field. However, for small deviations from exact alignment, typically less than ± 15 degrees for all the data presented in this paper, these errors can only be significant for waves propagating very nearly perpendicular to the geomagnetic field. Furthermore, the errors introduced by misalignment change sign as the satellite oscillates about its equilibrium orientation so that these errors can be recognized by looking for a systematic dependence of the correlation measurements on the satellite orientation relative to the geomagnetic field.

The actual correlation measurements are made on the ground using the wide-band analog electric and magnetic field signals transmitted from the satellite. These wide-band signals are filtered by an Ad-Yu Electronics Model 1034 Dual Channel Synchronous Filter to select the frequency at which the correlation of the two signals is to be determined (see Figure 2). The pass bands of the two narrow-band filter channels are identical, the center frequency of the two filter channels being determined by a single tuning oscillator and the bandwidth by plug-in units. A bandwidth of 50 Hz has been used for all measurements presented in this paper. The two narrow-band outputs from the synchronous filter then go to a four-quadrant analog multiplier which produces an output proportional to the algebraic product, $E_y B_z$, of the narrow-band E_y and B_z input signals. The analog multiplier output is then averaged by a simple R-C integrator with an R-C time constant of 50 milliseconds to give a good approximation to the time-averaged product $\langle E_y B_z \rangle$.

In the process of transmitting and demodulating the wide-band electric and magnetic field signals, various frequency-dependent phase shifts occur which must be corrected with a phase shift network prior to making a correlation measurement. Based on the reproducibility of various prelaunch calibrations, the overall uncertainty in

the phase shift corrections required is believed to be less than ± 5 degrees. To establish that errors of this magnitude do not affect the sign of the correlation measurement, we have required for all data presented that a phase shift of ± 10 degrees applied to one channel not change the sign of the correlation measurement.

The determination of the Poynting flux direction of proton whistlers provides a good check on the Poynting flux sensing technique, since proton whistlers (at higher latitudes) are known to be propagating upward from the base of the ionosphere [see Gurnett et al., 1965]. Figure 3 illustrates the determination of the Poynting flux direction for a series of proton whistlers. The Poynting flux is observed to be directed upward as expected. It should be noted here that $\langle E_y B_z \rangle$ differs from a correlation coefficient in that it is not normalized; hence the correlation levels for the various proton whistlers in Figure 3 depend on the intensity of the proton whistler signals.

III. INITIAL OBSERVATIONS

A. Reflection Phenomena

The determination of the Poynting flux by the methods described above is an especially good tool for the study of reflection phenomena. Figure 4 illustrates some discrete VLF emissions occurring in pairs, the two components of each pair being separated by a few tenths of a second. The correlation measurement clearly shows that the first emission in each pair is downgoing and the second emission is upgoing, indicating that the emissions have been reflected below the satellite altitude of approximately 1350 km. The delay times between the two components of each pair are consistent with a reflection at the base of the ionosphere below the satellite.

B. ELF Hiss

Illustrated in Figure 5 is an example of ELF hiss observed at an altitude of approximately 1200 km. From the correlation measurement at 600 Hz, the ELF hiss is clearly downgoing. Twelve examples of ELF hiss have been investigated to date at altitudes up to 1500 km and all have been found to be downgoing. This result is in agreement with previous evidence on the direction of propagation of ELF hiss [Gurnett and Burns, 1968]. No systematic dependence of the

correlation measurement on the satellite orientation was observed for any of the ELF hiss cases studied. It is thus concluded that errors in the magnetic alignment of the satellite did not affect the Poynting flux determination for ELF hiss.

Figure 5 also illustrates an ELF hiss correlation measurement at the sharp lower cutoff frequency (510 Hz) of the ELF hiss band. In this measurement, both downgoing and upgoing waves are observed with the upgoing component being less intense, indicating that reflections of the ELF hiss are occurring below the satellite. These observations are consistent with the explanation of the low-frequency cutoff of ELF hiss given by Gurnett and Burns [1968] in terms of reflections near the two-ion cutoff frequency. The correlation measurement at 600 Hz in Figure 5, showing only downgoing waves, suggests that the ELF hiss is not being reflected below the satellite altitude at this frequency. This can occur if the wave frequency is above the maximum two-ion cutoff frequency in the ionosphere at all altitudes below the satellite. The two-ion cutoff is seldom observed above 600-650 Hz [Gurnett and Burns, 1968] so that the ELF hiss at 600 Hz in Figure 5 is very likely above the maximum two-ion cutoff and is, therefore, able to propagate to the base of the ionosphere, where strong absorption can occur to attenuate the reflected wave.

C. Periodic Emissions

Figure 6 illustrates an example of periodic emissions in which all of the observed emissions are downgoing. These emissions were observed for a period of approximately three minutes over an altitude range of approximately 150 km and a range of magnetic shell parameters from $L = 4.2$ to $L = 3.6$. Since the echo period of the periodic emission is very nearly constant over this large range of L values, it is concluded that the observed emissions must have "leaked" from the L shell on which the echoing is taking place and propagated directly to the satellite. The observation in Figure 6 strongly supports this conclusion since no upgoing waves associated with the echoing process are observed.

D. VLF Hiss

Figure 7 shows a correlation measurement for auroral-zone VLF hiss. In this example, and in 15 additional examples which have been studied up to this time, VLF hiss is observed to be propagating down the geomagnetic field lines (in the northern hemisphere). However, in all but 2 of the 16 cases observed, there are also some brief impulsive bursts propagating up the geomagnetic field lines from below the satellite. The upgoing signals are much less intense than the downgoing signals and the impulsive bursts which characterize many of the VLF hiss events are much less frequent for the upgoing waves than for the downgoing waves.

These observations suggest that VLF hiss is generated above the altitude range of the Injun 5 satellite. The occasional upgoing VLF hiss bursts which are observed are believed to be reflections of downgoing waves below the satellite near the altitude at which the wave frequency equals the lower-hybrid-resonance (LHR) frequency. The reflection mechanism at the LHR frequency has been discussed by Thorne and Kennel [1967] and Storey and Cerisier [1968], who show that downgoing waves with wave normal angles near $\pi/2$ will be reflected when the wave frequency becomes less than the LHR frequency.

No orientation dependence has been observed in any of the cases of VLF hiss studied up to this time. It is concluded, therefore, that the misorientation of the satellite is also not affecting the Poynting flux determinations of VLF hiss.

E. Chorus

Very few examples of chorus have been analyzed up to this time so that definite conclusions regarding the source region of chorus cannot be presented. Figure 8 illustrates one measurement which has been made and which shows the chorus to be downgoing at the satellite altitude of approximately 2500 km. Additional cases of chorus must be studied before any definite conclusions can be made.

F. Saucer-Shaped Emissions

Illustrated in Figure 9 is a new type of emission which is called a "saucer," following the established terminology of several investigators [personal communication, N. Brice, R. L. Smith, R. E. Barrington]. In contrast to all other types of emissions investigated to date, the Poynting flux of the saucer-shaped emission is directed up the geomagnetic field line, indicating that the source of the emission is below the satellite. The satellite altitude for the event shown in Figure 9 is 2530 km and the invariant latitude is 69.8°.

Saucer-shaped emissions of the type shown in Figure 9 were first observed with the Alouette 1 and 2 satellites [R. E. Barrington, personal communication] and are commonly observed at high latitudes near the auroral zone with the Injun 5 satellite. These emissions typically have a duration from several seconds to several tens of seconds and occur in the frequency range from about 2 kHz to above 10 kHz. The outer "envelope" of the emission is often sharply defined, as for the case shown in Figure 9, and the electric field intensity is usually greater than the magnetic field intensity, on a free space basis. In addition, spectrograms of these emissions sometimes have attenuation bands at harmonics of the proton gyrofrequency [see Figure 14 of Gurnett et al., 1969].

V-shaped VLF hiss events, similar in some respects to the saucer-shaped emissions reported here but usually of much longer duration (~ 100 seconds) have been previously studied and reported by Gurnett [1966]. Because of their much longer duration, the V-shaped VLF hiss emissions are believed to be distinctly different from, although possibly related to, the saucer-shaped emissions of the type shown in Figure 9. The Injun 3 data [Gurnett, 1966] showed that the V-shaped VLF hiss events were often associated with intense fluxes of soft (10 keV) electrons, with the VLF emission usually being symmetric in latitude about the region of most intense electron flux.

The symmetry of the saucer envelope suggests that the source of this emission may also lie along the symmetry axis of the emission, much as for the V-shaped VLF hiss events. Unfortunately, because of the limited data available at the time of this preliminary report, the relationship between the saucer-shaped emissions and charged particle fluxes simultaneously observed with Injun 5 has not yet been investigated.

IV. A QUALITATIVE EXPLANATION OF THE SAUCER ENVELOPE

When the anisotropic propagation of whistler-mode waves upward from a source below the satellite is considered, a ready explanation arises for the characteristic frequency-time spectra of the saucer-shaped emissions. For a qualitative model we visualize the source as being along an east-west line (an auroral arc, for example) far below the satellite. The sharply defined frequency-time envelope of the saucer can then be explained by a frequency-dependent limiting ray angle for propagation from the source to the satellite. The noise intensity variations observed at a given frequency are completely due to the horizontal (north-south) motion of the satellite through the "beam" of allowed ray paths from the source to the satellite, and the frequency dependence of the beamwidth accounts for the observed frequency-time envelope of the emission.

For the whistler mode of propagation there are two limiting ray angles which could possibly explain the observed beamwidth. As shown by Smith [1960], Helliwell [1965] and others, the angle ψ between the ray direction and the static magnetic field depends on the wave normal angle θ , also measured relative to the static magnetic field, as shown in Figure 10(a). The first limiting ray angle, ψ_{\max} , occurs

at a wave normal angle intermediate between $\theta = 0$ and $\theta = \theta_{\text{res}}$. This first limiting ray angle was originally discussed by Storey [1953] in connection with the guiding of whistlers in the geomagnetic field. In the low frequency limit ψ_{max} is approximately $19^\circ 29'$ [Storey, 1953]. The second limiting ray angle, ψ_{res} , occurs as the refractive index goes to infinity at a wave normal angle equal to the resonance cone angle, θ_{res} . Since the ray direction is perpendicular to the refractive index surface [Stix, 1962], the simple geometric construction in Figure 10(b) shows that $\psi_{\text{res}} = \pi/2 - \theta_{\text{res}}$.

Several factors strongly suggest that it is this second limiting ray angle, ψ_{res} , for wave normal angles near the resonance cone angle, which accounts for the characteristic shape of the saucer envelope: (1) Since the temporal (spatial) width of the envelope increases with increasing frequency, the limiting ray angle must increase with increasing frequency. Only ψ_{res} has the required frequency dependence since ψ_{max} decreases with increasing frequency [see Smith, 1960]. (2) The large observed ratio of electric to magnetic field strengths for the saucer-shaped emissions suggests that the wave normal angle is very close to the resonance cone angle. (3) The proton cyclotron harmonic interactions observed and the doppler shifting of the cyclotron harmonic frequencies sometimes observed [Gurnett et al., 1969] suggest that the wavelengths

involved may be as short as 100 meters, corresponding to a very large refractive index (~ 300). These very short wavelengths are possible only for wave normal angles near the resonance cone angle.

Wave normal angles very near the resonance cone angle could occur because of several possible reasons. The emission mechanism may favor the production of waves with wave normal angles near the resonance cone angle. Also, even for wave normal angles not initially near the resonance cone angle the rapid decrease in the electron density and refractive index with increasing altitude by Snell's law causes the wave normal angle to approach the resonance cone angle as the wave propagates upward through the ionosphere.

The qualitative explanation of the frequency-time shape of the saucer-shaped emission is illustrated in Figures 10(c) and 10(d) which show the limiting ray paths from the source to the satellite at several frequencies and the resulting frequency-time spectrogram observed by the satellite passing over the source. For this qualitative illustration, we have assumed that the plasma parameters are independent of altitude so that the ray paths are straight lines. A more quantitative model would of course require a detailed ray path integration.

The simple ray path model illustrated in Figure 10 qualitatively explains the principal features of the saucer

emission envelope: (1) All waves with wave normal angles near the resonance cone angle result in ray paths which are inside the limiting ray path and, hence, inside the outer envelope of the emission. The large field intensity near the envelope is the result of the very small spread in ray directions for wave normal directions near the resonance cone angle. (2) The frequency-time shape of the outer envelope can be understood in terms of the frequency dependence of the limiting ray angle, ψ_{res} . Using the notation defined by Stix [1962], the limiting ray angle is given by

$$\tan^2 \psi_{\text{res}} = \frac{-S}{P} . \quad (1)$$

If x is the horizontal distance (also proportional to the time coordinate on the spectrogram) from the symmetry axis of the emission and h is the altitude of the satellite above the source, then

$$\left(\frac{x}{h}\right)^2 = \tan^2 \psi_{\text{res}} = \frac{-S}{P} . \quad (2)$$

The minimum frequency of the emission envelope ($x = 0$) can now be identified as the lower-hybrid-resonance (LHR) frequency, where $S = 0$ [see Stix, 1962]. The shape of the emission envelope near the LHR frequency can be approximated by expanding S in a Taylor series about $f = f_{\text{LHR}}$ and neglecting higher order terms

$$S = \frac{\partial S}{\partial f} (f - f_{LHR}) ,$$

which upon substituting into equation 2 becomes

$$\left(\frac{x}{h}\right)^2 = \frac{-\partial S / \partial f}{P} (f - f_{LHR}) . \quad (3)$$

Equation 3 above shows that in the neighborhood of the LHR frequency, where $\partial S / \partial f$ and P can be regarded as constant, the emission envelope is a parabola.

At higher frequencies the shape of the emission envelope depends on the detailed plasma parameters. If the electron plasma frequency, f_p , is less than the electron gyrofrequency, f_g , then the envelope asymptotically approaches the electron plasma frequency as shown in Figure 10, since P goes to zero at $f=f_p$. If f_p is greater than f_g , then the envelope asymptotically approaches the electron gyrofrequency, since S becomes infinite at $f=f_g$. Thus, the upper frequency limit is either f_p or f_g , whichever is smaller. Since the upper frequency limit of the Injun 5 wideband receiver is well below either the electron gyrofrequency or plasma frequency, the flaring of the emission envelope at high frequencies, as shown in Figure 10(d), has not yet been experimentally verified.

To provide a rough quantitative verification of this explanation of the emission envelope shape, equation 2 was fit to the envelope of the saucer shown in Figure 9, even though this equation was derived under the rather unrealistic assumption of a completely homogeneous ionosphere with straight-line ray paths. The electron gyrofrequency at the satellite during this event was determined to be $f_g = 602$ kHz from the Jensen and Cain [1962] expansion for the geomagnetic field, and the electron plasma frequency was determined to be $f_p = 200$ kHz from the AFCRL electron density probe on Injun 5 [personal communication, R. Sagalyn]. For these rather low density conditions, with $f_p^2 \ll f_g^2$, S in equation 2 can to a very good approximation be written.

$$S = 1 - \frac{f_{LHR}^2}{f^2} .$$

Since $P = 1 - f_p^2/f^2$ [Stix, 1962], Equation 2 becomes

$$\left(\frac{x}{h}\right)^2 = \frac{f^2 - f_{LHR}^2}{f_p^2 - f^2} . \quad (4)$$

Using $f_p = 200$ kHz and $f_{LHR} = 1.7$ kHz (estimated from the minimum frequency of the emission envelope), equation 4 above was found to provide an excellent fit to the envelope of the saucer shown in Figure 9 if the source were located at

$h = 1100$ km below the satellite or at an altitude of about 1400 km. Since this source location assumed straight-line ray paths, it should be emphasized that this calculation gives a "virtual source location" which may differ somewhat from the actual source location when vertical gradients in the ionosphere are considered. Nevertheless, the excellent agreement between the observed shape of the emission envelope and equation 4 and the physically reasonable virtual source altitude predicted shows that this proposed explanation of the saucer envelope is quantitatively reasonable.

When vertical gradients in the ionosphere are considered, the detailed shape of the emission envelope must, in general, be determined by numerical integration. If the electron plasma frequency and the lower-hybrid-resonance frequency decrease monotonically with increasing altitude as shown in Figure 11(a), then the limiting ray paths and the corresponding emission envelope will have the form illustrated in Figures 11(b) and 11(c). The altitude dependence of the plasma frequency causes the ray paths to diverge as illustrated in Figure 11(b) because ψ_{res} increases with increasing altitude. This divergence has the effect of lowering the source altitude below the source altitude computed using equation 4.

The low-frequency cutoff at f_{LHR} (source) occurs because there is no limiting ray path ($\tan^2 \psi_{res}$ is negative) for altitudes where the wave frequency is less than the LHR

frequency. The gap in the emission envelope at f_{LHR} (source) occurs because the two limiting ray paths at this frequency diverge as they propagate upward into the ionosphere. For frequencies below the LHR frequency, the ray paths are a sensitive function of the initial wave normal angle and no general statements can be made concerning limiting ray paths at these frequencies.

Effects due to this "gap" in the emission envelope are often clearly evident in the saucer-shaped emissions observed with Injun 5. Near the minimum frequency of the emission the envelope often becomes very indistinct and poorly defined, as can be seen for the saucer shown in Figure 9. In some cases the emission almost completely disappears in the gap region as could be expected from the ray path model illustrated in Figure 11.

This propagation model accounts for most of the general characteristics of the saucer-shaped emissions, and is believed to be essentially correct. However, many detailed questions remain to be investigated, including (1) the actual source altitude, (2) the source geometry (point, line, sheet or extended source), (3) the emission mechanism and related particle fluxes, and (4) the detailed origin of the proton cyclotron harmonics sometimes observed.

IV. SUMMARY

The results presented above are preliminary in that only a small portion of the Injun 5 data has been studied. However, several conclusive results have been obtained from these data. ELF hiss has been observed to be downgoing at altitudes below 1500 km and VLF hiss has been observed as generally downgoing with some upgoing waves at altitudes up to 2500 km, indicating that the sources of these emissions exist above these altitudes.

At the time of this report, the only observed phenomenon which appears to be generated below the satellite altitude is the saucer-shaped emission. The characteristic frequency-time shape of this emission has been explained as a propagation effect for whistler-mode waves propagating upward from the source to the satellite.

It should be commented that the results presented in this paper represent only an initial study of a small amount of data so that broad generalizations of these results may not be justified. Further studies investigating all altitude, latitude, and local times covered by Injun 5 and considering possible subcategories of various phenomena are planned and will be presented at the earliest possible time.

ACKNOWLEDGEMENTS

The authors wish to express their thanks to Mr. G. W. Pfeiffer, Mr. D. Odem, and Mr. R. R. Anderson for their considerable effort in testing and calibrating this experiment, and to all the personnel involved in the Injun 5 project for their effort in making this experiment a success. We also wish to thank Dr. R. Sagalyn for her effort in providing electron density data.

This research was supported in part by the National Aeronautics and Space Administration under Contracts NAS5-10625, NAS1-8141, NAS1-8144(f), NAS1-8150(f), and NGR-16-001-043; and by the Office of Naval Research under Contract Nonr 1509(06).

REFERENCES

- Gurnett, D. A., "A satellite study of VLF hiss," J. Geophys. Res., 71, 5599, 1966
- Gurnett, D. A., S. D. Shawhan, N. M. Brice, and R. L. Smith, "Ion cyclotron whistlers," J. Geophys. Res., 70, 1665 1965.
- Gurnett, D. A. and T. B. Burns, "The low-frequency cutoff of ELF emissions," J. Geophys. Res., 73, 7437, 1968.
- Gurnett, D. A., G. W. Pfeiffer, R. R. Anderson, S. R. Mosier, and D. P. Cauffman, "Initial observations of VLF electric and magnetic fields with the Injun 5 satellite," J. Geophys. Res., in press, 1969.
- Helliwell, R. A., Whistlers and Related Ionospheric Phenomena, Stanford University Press, 1965.
- Jensen, D. C. and J. C. Cain, "An interim geomagnetic field" (abstract), J. Geophys. Res., 67, 3568, 1962.
- Smith, R. L., "Guiding of whistlers in a homogeneous medium," J. Res. Nat. Bureau of Standards, D. Radio Propagation, 64D(5), 505, 1960.
- Stix, T. H., The Theory of Plasma Waves, McGraw-Hill Book Company, New York, 1962.
- Storey, L. R. O., "An investigation of whistling atmospherics," Phil. Trans. Roy. Soc. [A], 246, 113, 1953.

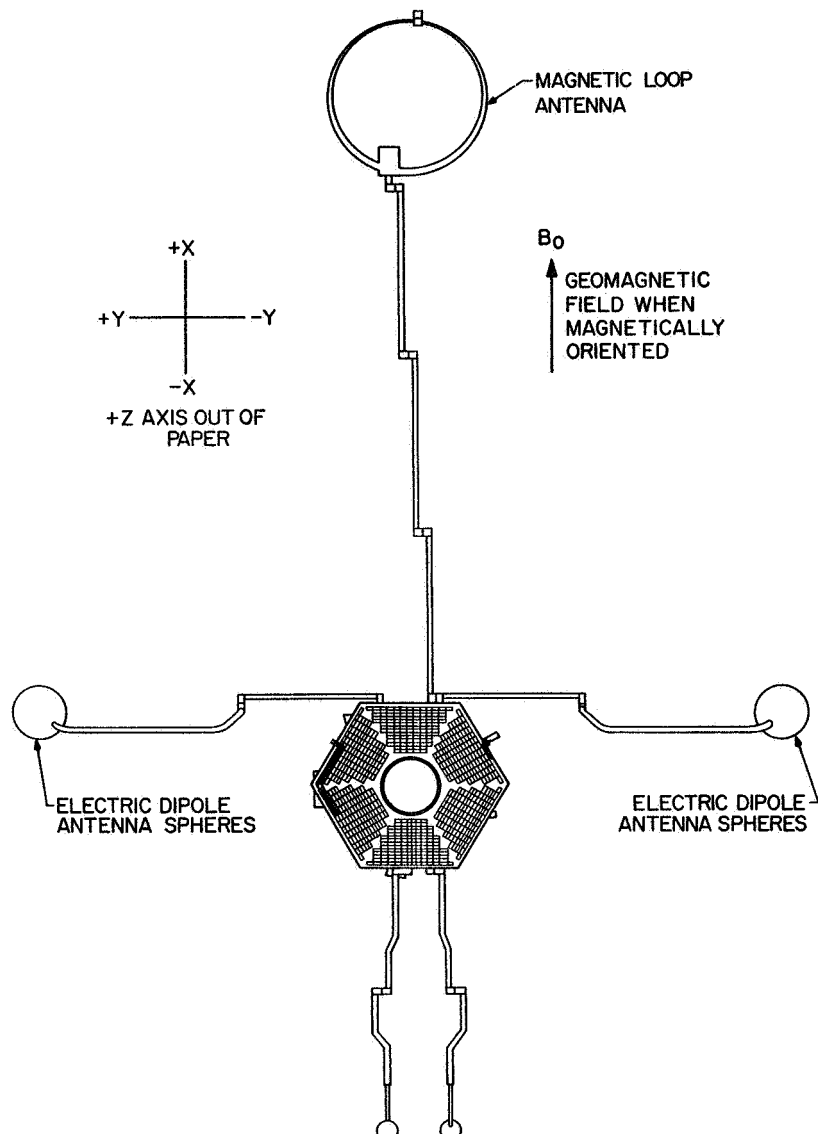
Storey, L. R. O., and J. C. Cerisier, "An interpretation of the noise bands observed near the lower hybrid resonance frequency by artificial satellites, C. R. Acad. Sc. Paris, t.266, 525, 1968.

Thorne, R. M. and C. F. Kennel, "Quasi-trapped VLF propagation in the outer magnetosphere," J. Geophys. Res., 72, 857, 1967.

FIGURE CAPTIONS

- Figure 1 Top view of the Injun V satellite showing the orientation of the electric dipole and magnetic loop antenna.
- Figure 2 Block diagram of the instrumentation used to determine the direction of the Poynting flux along the geomagnetic field.
- Figure 3 Correlation measurement of a group of proton whistlers.
- Figure 4 Correlation measurement of discrete VLF emissions.
- Figure 5 Correlation measurement of ELF hiss.
- Figure 6 Correlation measurement of periodic emission.
- Figure 7 Correlation measurement of VLF hiss.
- Figure 8 Correlation measurement of VLF chorus.
- Figure 9 Correlation measurement of saucer-shaped emission.
- Figure 10 Ray paths for the saucer-shaped emission in a homogeneous ionosphere.
- Figure 11 Ray paths including the effect of a vertical gradient in the ionosphere.

G68-1050-I



0 1 2 3 4 5 6
FEET

TOP VIEW
OF INJUN ∇

Figure 1

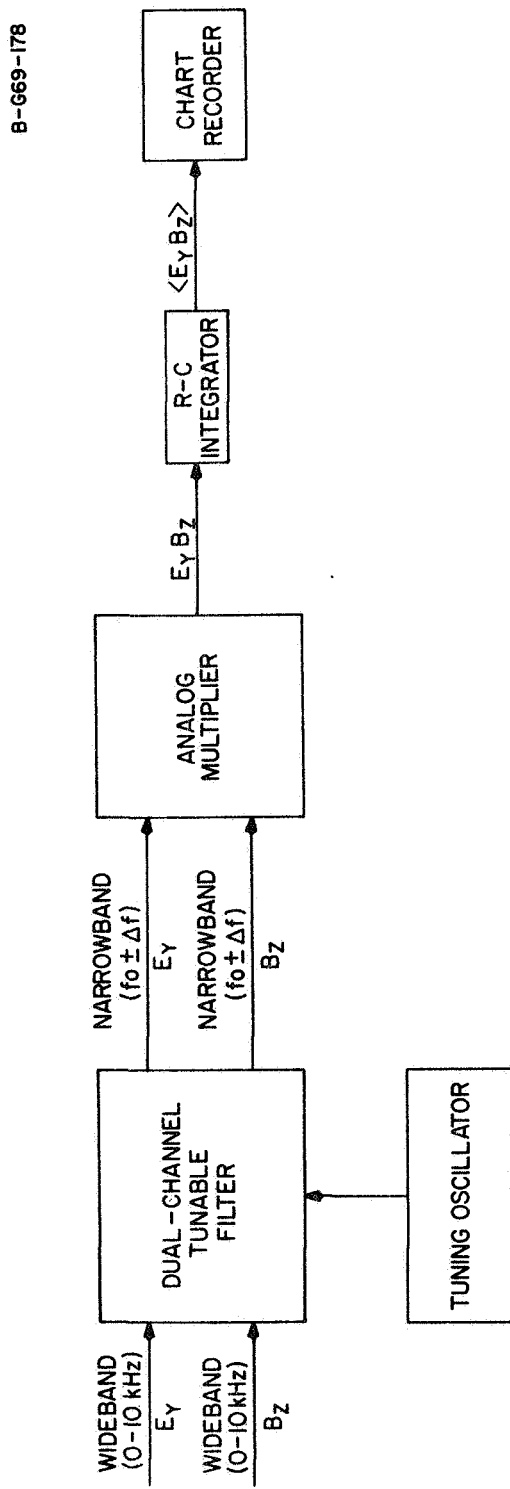


Figure 2

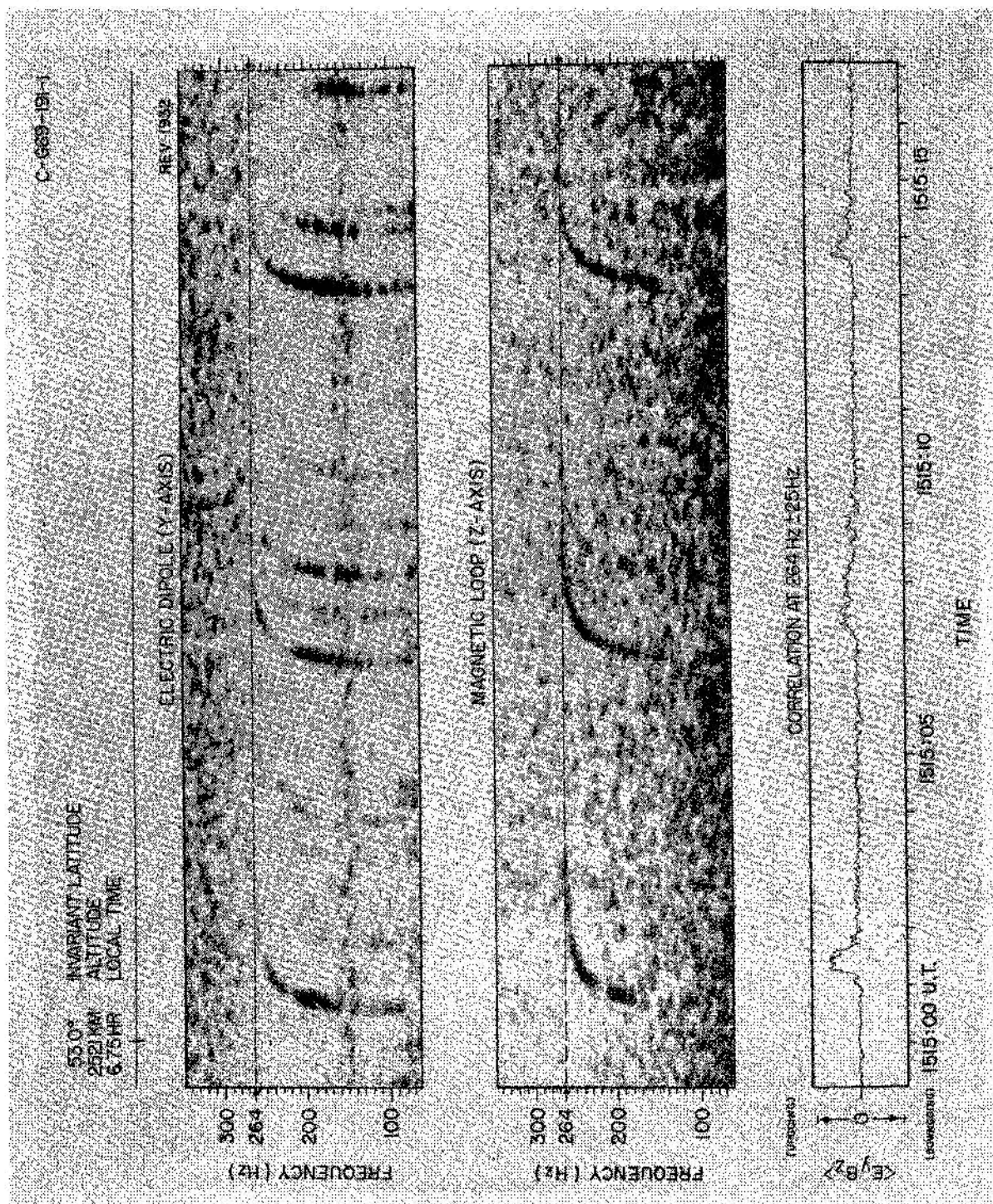


Figure 3

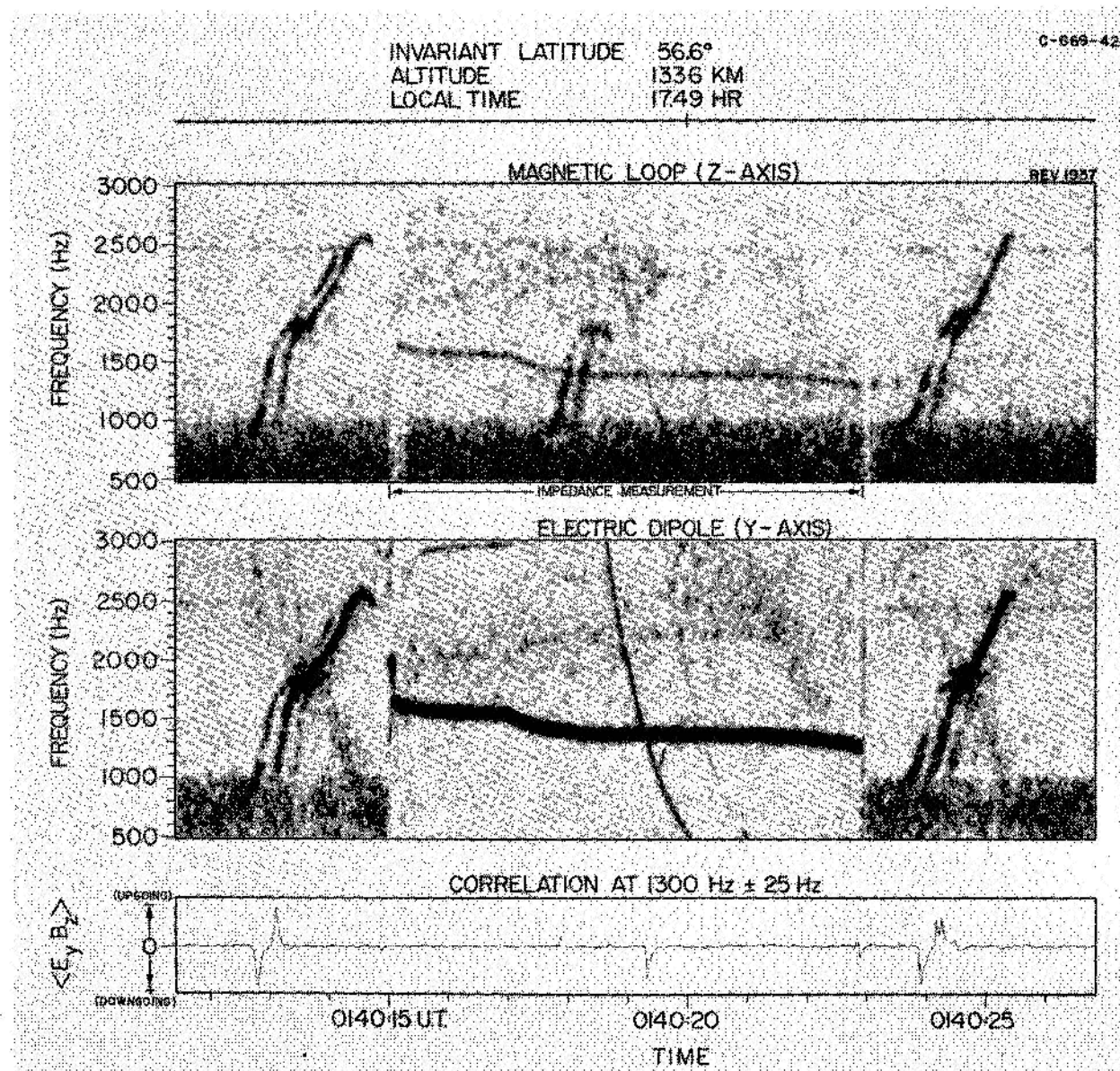


Figure 4

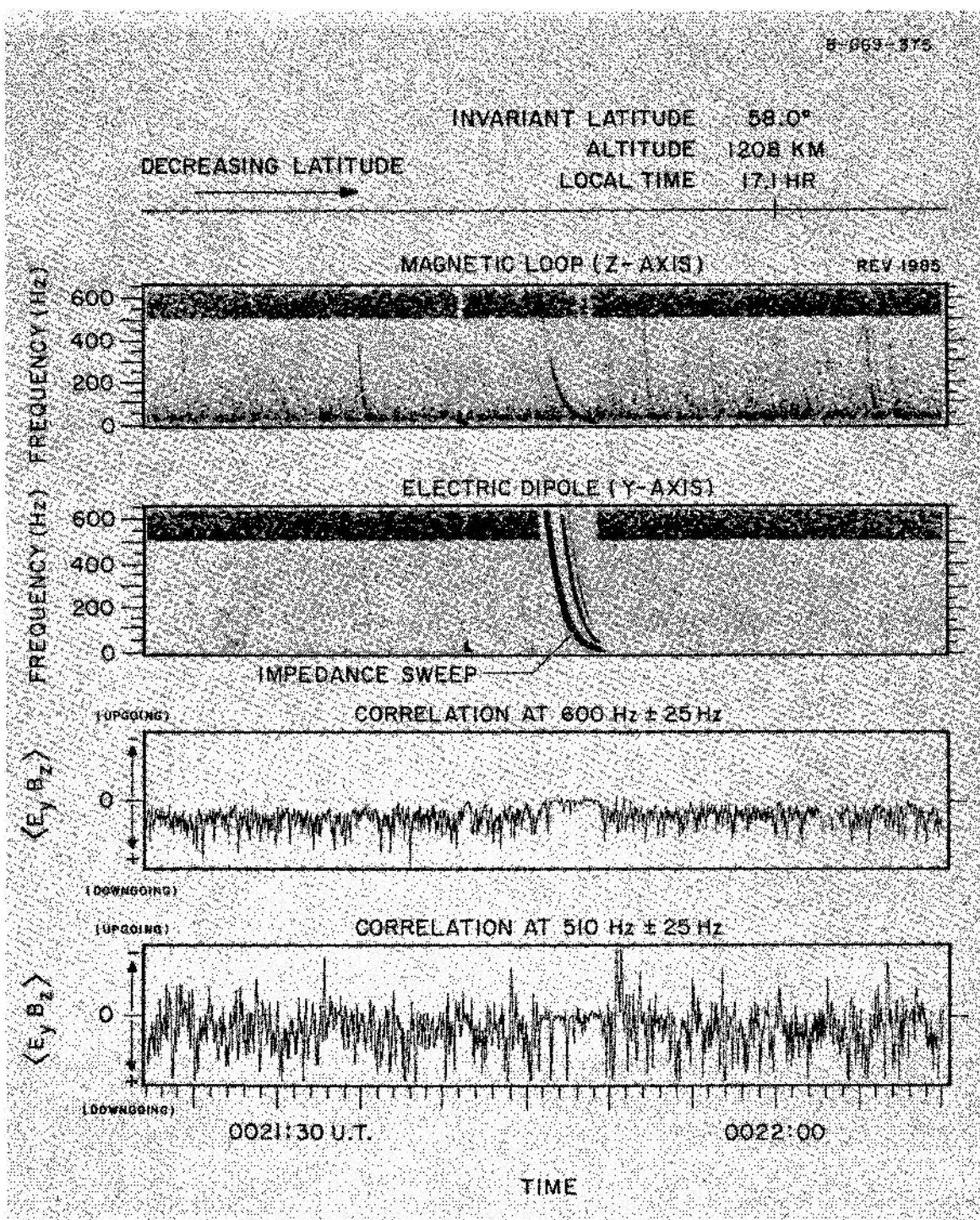


Figure 5

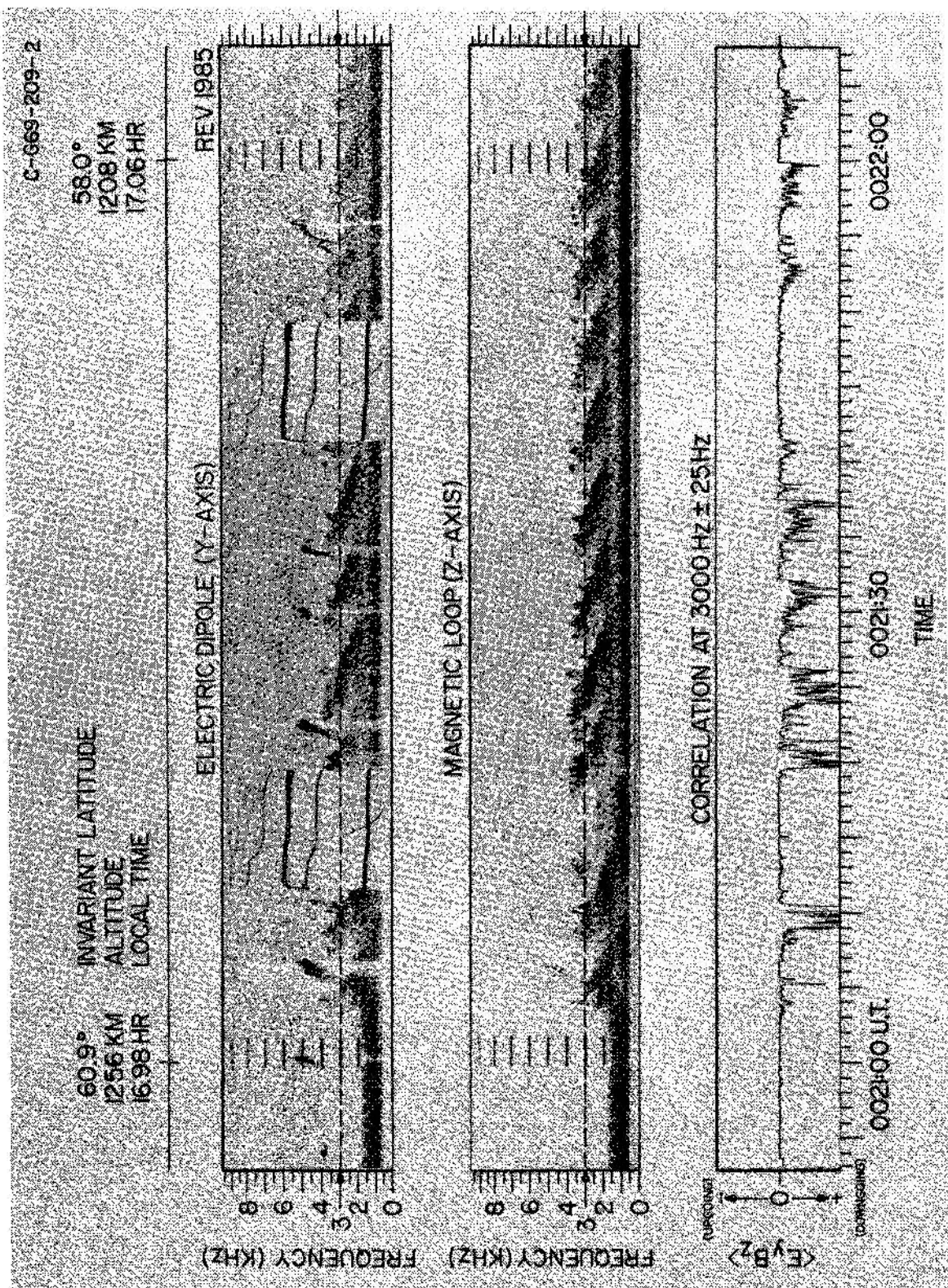


Figure 6

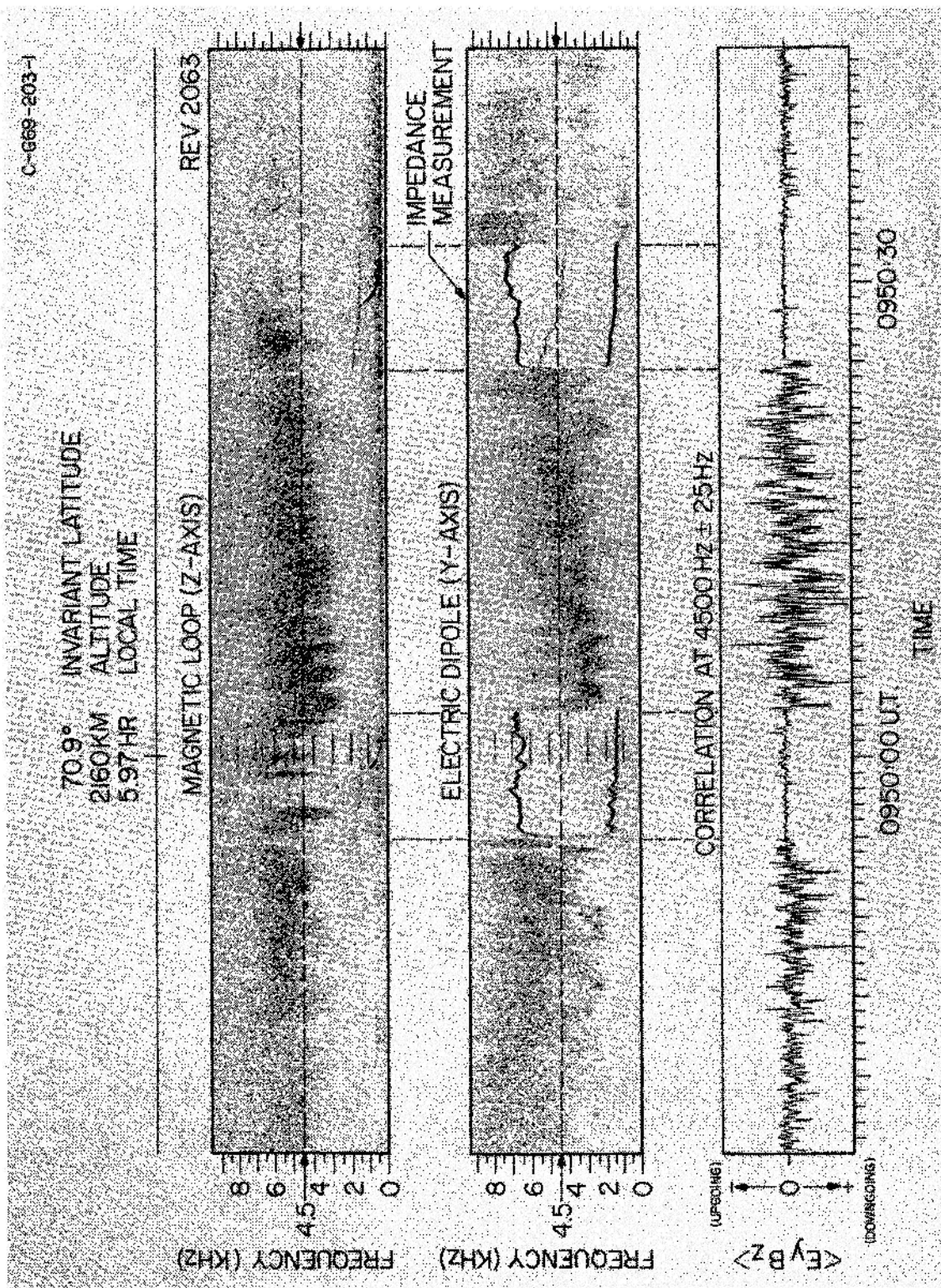


Figure 7

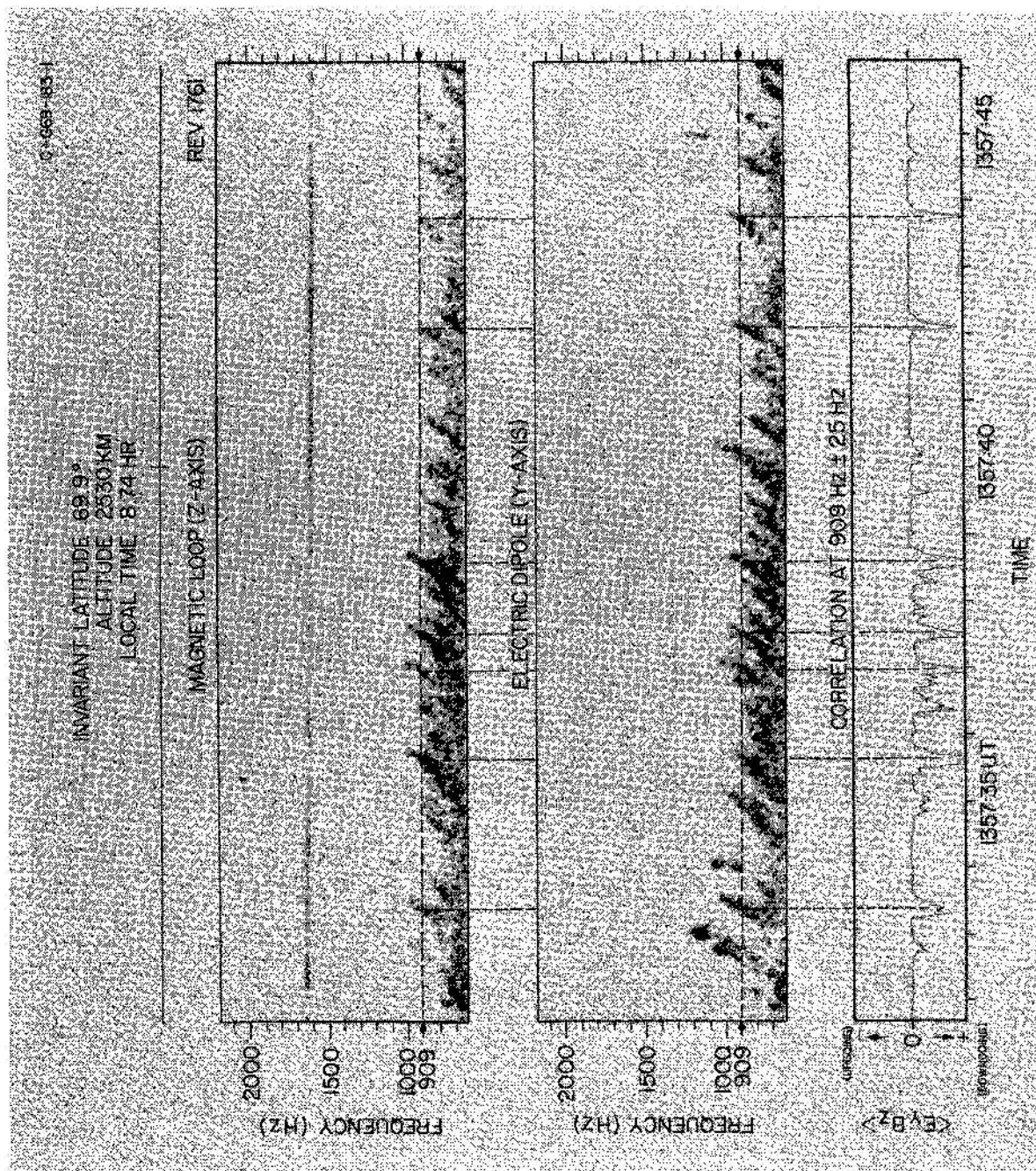


Figure 8

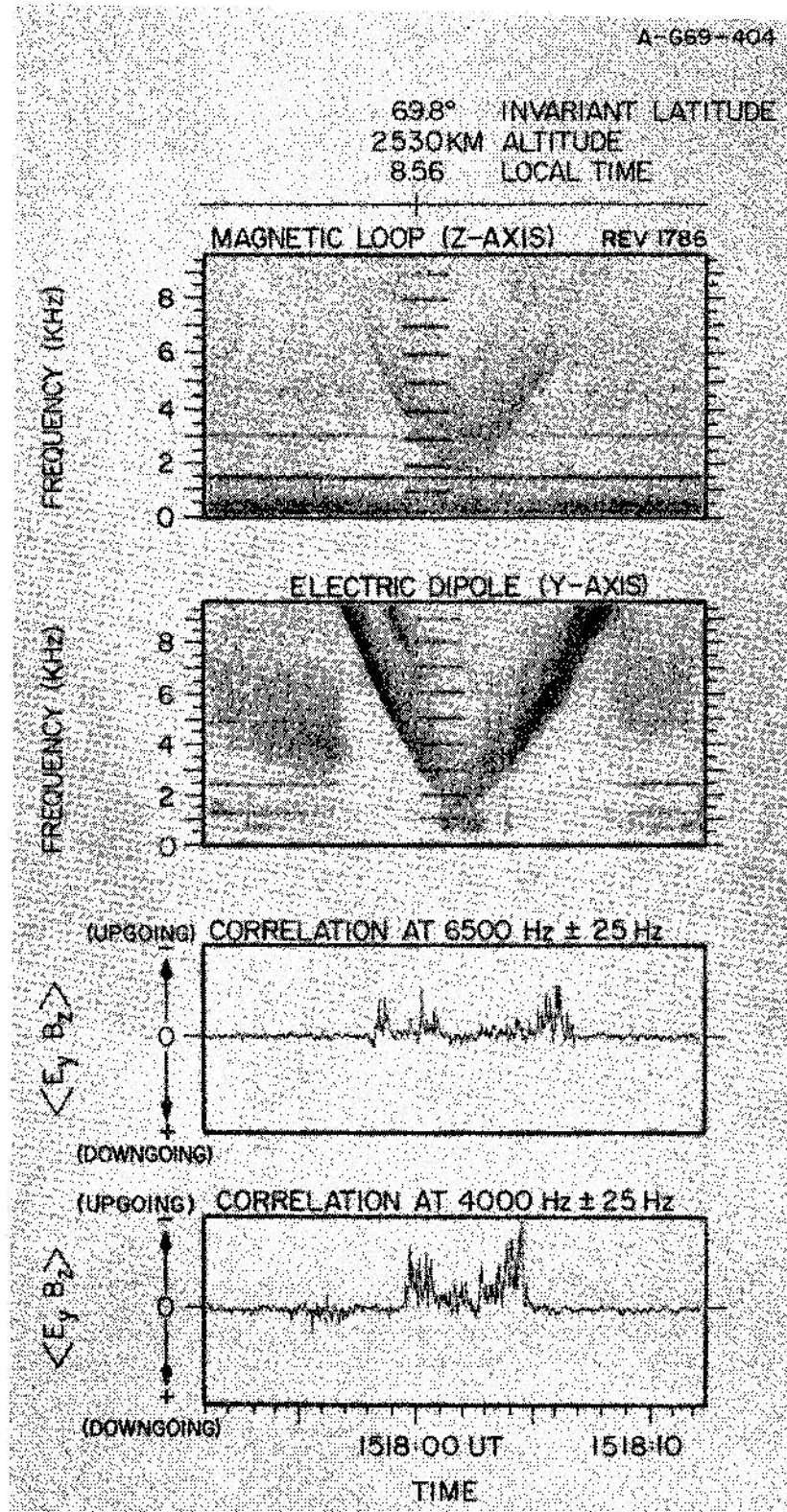


Figure 9

D-669-455-1

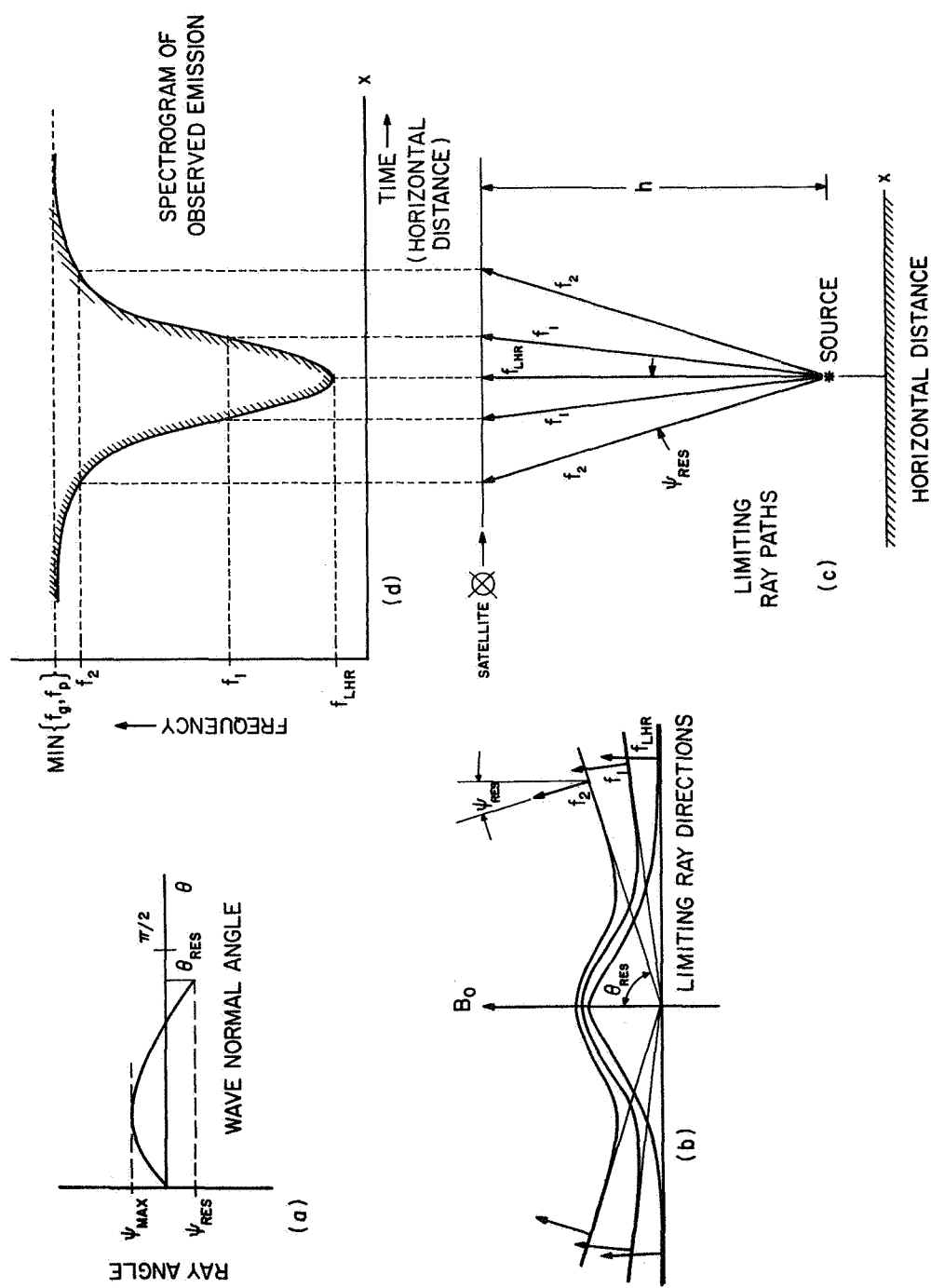


Figure 10

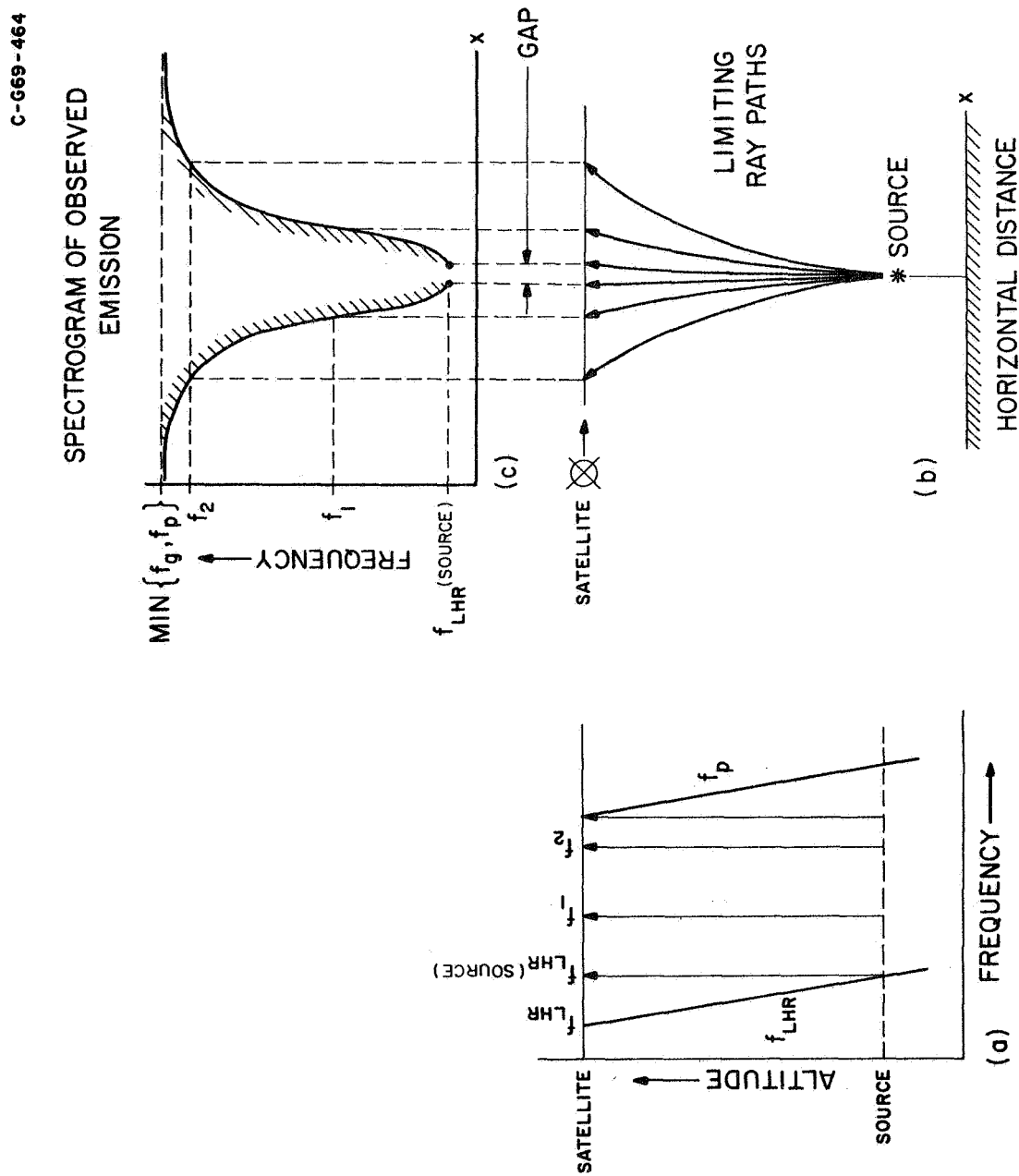


Figure 11

UNCLASSIFIED

Security Classification

DOCUMENT CONTROL DATA - R&D

(Security classification of title, body of abstract and indexing annotation must be entered when the overall report is classified)

1. ORIGINATING ACTIVITY (Corporate author) The University of Iowa, Department of Physics and Astronomy	2a. REPORT SECURITY CLASSIFICATION UNCLASSIFIED
2b. GROUP	

3. REPORT TITLE

VLF Measurements of the Poynting Flux along the Geomagnetic Field with the Injun 5 Satellite

4. DESCRIPTIVE NOTES (Type of report and inclusive dates)

Progress report June 1969

5. AUTHOR(S) (Last name, first name, initial)

Mosier, Stephen R., Gurnett, Donald A.

6. REPORT DATE April June 1969	7a. TOTAL NO. OF PAGES 38	7b. NO. OF REFS 11
8a. CONTRACT OR GRANT NO. Nonr 1509(06)	9a. ORIGINATOR'S REPORT NUMBER(S) U. of Iowa 69-27	
b. PROJECT NO. c. d.	9b. OTHER REPORT NO(S) (Any other numbers that may be assigned this report)	

10. AVAILABILITY/LIMITATION NOTICES

Distribution of this document is unlimited.

11. SUPPLEMENTARY NOTES	12. SPONSORING MILITARY ACTIVITY Office of Naval Research
-------------------------	--

13. ABSTRACT

The direction of the Poynting flux, up or down the geomagnetic field, has been determined for several types of VLF radio noise phenomena observed with the Injun 5 satellite, thereby providing information about the source region of these waves and their propagation in the ionosphere. Determinations of the Poynting flux direction of proton whistlers show that they are propagating up the geomagnetic field lines in accordance with the accepted theory of proton whistler propagation, thus providing a good check on the experimental technique. Initial measurements are presented on the Poynting flux direction of the ELF hiss, periodic emissions, VLF hiss, and chorus. Of particular interest is a new type of VLF emission called a saucer which is found to be propagating upward from a source below the satellite. A qualitative explanation of the frequency-time shape of this new type of emission is presented.

UNCLASSIFIED

Security Classification

14.	KEY WORDS	LINK A		LINK B		LINK C	
		ROLE	WT	ROLE	WT	ROLE	WT
	VLF Measurements, Poynting Flux Along Geomagnetic Field, Injun 5 Satellite						

INSTRUCTIONS

1. ORIGINATING ACTIVITY: Enter the name and address of the contractor, subcontractor, grantee, Department of Defense activity or other organization (*corporate author*) issuing the report.

2a. REPORT SECURITY CLASSIFICATION: Enter the overall security classification of the report. Indicate whether "Restricted Data" is included. Marking is to be in accordance with appropriate security regulations.

2b. GROUP: Automatic downgrading is specified in DoD Directive 5200.10 and Armed Forces Industrial Manual. Enter the group number. Also, when applicable, show that optional markings have been used for Group 3 and Group 4 as authorized.

3. REPORT TITLE: Enter the complete report title in all capital letters. Titles in all cases should be unclassified. If a meaningful title cannot be selected without classification, show title classification in all capitals in parenthesis immediately following the title.

4. DESCRIPTIVE NOTES: If appropriate, enter the type of report, e.g., interim, progress, summary, annual, or final. Give the inclusive dates when a specific reporting period is covered.

5. AUTHOR(S): Enter the name(s) of author(s) as shown on or in the report. Enter last name, first name, middle initial. If military, show rank and branch of service. The name of the principal author is an absolute minimum requirement.

6. REPORT DATE: Enter the date of the report as day, month, year; or month, year. If more than one date appears on the report, use date of publication.

7a. TOTAL NUMBER OF PAGES: The total page count should follow normal pagination procedures, i.e., enter the number of pages containing information.

7b. NUMBER OF REFERENCES: Enter the total number of references cited in the report.

8a. CONTRACT OR GRANT NUMBER: If appropriate, enter the applicable number of the contract or grant under which the report was written.

8b, 8c, & 8d. PROJECT NUMBER: Enter the appropriate military department identification, such as project number, subproject number, system numbers, task number, etc.

9a. ORIGINATOR'S REPORT NUMBER(S): Enter the official report number by which the document will be identified and controlled by the originating activity. This number must be unique to this report.

9b. OTHER REPORT NUMBER(S): If the report has been assigned any other report numbers (*either by the originator or by the sponsor*), also enter this number(s).

10. AVAILABILITY/LIMITATION NOTICES: Enter any limitations on further dissemination of the report, other than those imposed by security classification, using standard statements such as:

- (1) "Qualified requesters may obtain copies of this report from DDC."
- (2) "Foreign announcement and dissemination of this report by DDC is not authorized."
- (3) "U. S. Government agencies may obtain copies of this report directly from DDC. Other qualified DDC users shall request through ."
- (4) "U. S. military agencies may obtain copies of this report directly from DDC. Other qualified users shall request through ."
- (5) "All distribution of this report is controlled. Qualified DDC users shall request through ."

If the report has been furnished to the Office of Technical Services, Department of Commerce, for sale to the public, indicate this fact and enter the price, if known.

11. SUPPLEMENTARY NOTES: Use for additional explanatory notes.

12. SPONSORING MILITARY ACTIVITY: Enter the name of the departmental project office or laboratory sponsoring (*paying for*) the research and development. Include address.

13. ABSTRACT: Enter an abstract giving a brief and factual summary of the document indicative of the report, even though it may also appear elsewhere in the body of the technical report. If additional space is required, a continuation sheet shall be attached.

It is highly desirable that the abstract of classified reports be unclassified. Each paragraph of the abstract shall end with an indication of the military security classification of the information in the paragraph, represented as (TS), (S), (C), or (U).

There is no limitation on the length of the abstract. However, the suggested length is from 150 to 225 words.

14. KEY WORDS: Key words are technically meaningful terms or short phrases that characterize a report and may be used as index entries for cataloging the report. Key words must be selected so that no security classification is required. Identifiers, such as equipment model designation, trade name, military project code name, geographic location, may be used as key words but will be followed by an indication of technical context. The assignment of links, roles, and weights is optional.